Analysis of Piezoelectric Smart Composites Using a Coupled Piezoelectric-Mechanical Model

XU ZHOU, ADITI CHATTOPADHYAY* AND ROB THORNBURGH

Department of Mechanical and Aerospace Engineering, Arizona State University, Tempe, AZ 85287-6106

ABSTRACT: A two-way piezoelectric-mechanical coupled theory is used to investigate the multiple field interactions of composite laminates with surface-bonded piezoelectric actuators and sensors. A higher order electrical potential field is used to accurately describe the nonuniform distribution of electric potential through the thickness of piezoelectric layers. A higher order laminate theory is used to describe the displacement fields of both composite laminate and piezoelectric layers to accurately model transverse shear deformation which is significant in moderately thick constructions. A finite element laminate model with surface bonded/embedded piezoelectric actuators or sensors is developed to implement the theory. Induced deformation, charge and current are investigated to evaluate actuation and sensing effects of piezoelectric materials. The results obtained using this coupled theory are compared with those obtained using an uncoupled theory. Numerical results indicate that two-way coupling effects affect the prediction of structural deflection, stress distribution and electrical signal significantly. The thickness ratio of piezoelectric layer to plate structure is a critical parameter that governs the significance of coupling effects. The coupled piezoelectric-mechanical theory is capable of accurately modeling the characteristics of thick piezoelectric layers.

INTRODUCTION

THE development of smart composites offers great potential for advanced aerospace structural applications. Piezoelectric materials are employed as both actuators and sensors in the development of these structures by taking advantage of direct and converse piezoelectric effects. The modeling of laminated structures with surface-bonded piezoelectric transducers can be enhanced in two ways, more accurate mechanics model to address the characteristics of composite laminates and more accurate piezoelectric material model to address electrical characteristics and coupling effects between mechanical and electrical fields of actuators and sensors.

In the analysis of laminated structures using piezoelectric materials, the classical laminate theory (CLT) which ignores the transverse shear effects has been used extensively (Crawley, 1987; Lee, 1990). A refined hybrid plate theory that combines the layerwise theory and an equivalent single-layer theory (ESL) along with linear piezoelectricity was developed by Mitchell and Reddy (1995) to model smart composite laminates. A higher order theory that proved to be computationally more efficient and was capable of accurately capturing the transverse shear effects, for both thin and thick laminates, was developed by Chattopadhyay and Gu (1994). The effectiveness of the theory has been illustrated in the analysis of composite laminated structures (Chattopadhyay and Seeley, 1997; McCarthy and Chattopadhyay, 1997).

*Author to whom correspondence should be addressed. E-mail: aditi@asu.edu

In the study of actuation and sensing effects of piezoelectric materials, two way coupling, which implies the mutual interactions between piezoelectric and mechanical fields (both direct and converse piezoelectric effects), plays an important role (Tiersten, 1969). However, this issue is ignored in most applications. In most of the work (Detwiler et al. 1995; Cho and Parmerter, 1999; Chattopadhyay, Gu, and Dragomir-Daescu, 1999), a one-way coupling, that only considers either actuation effect (converse piezoelectric effect) of known electrical field on mechanical field or sensing effect (piezoelectric effect) of known mechanical field on electrical field, is used. Two-way coupling effects have been used by Hagood and Von Flotow (1991) in the study of passive electrical damping and later in the study of self-sensing actuators (Anderson and Hagood, 1994). The two-way coupling between piezoelectric and mechanical fields was included in the hybrid plate theory developed by Mitchell and Reddy (1995). Recently, a coupled thermal-piezoelectric-mechanical model was developed in Chattopadhyay, Li, and Gu (1999) and Gu et al., Zhou et al. (both in press), to address the two-way coupling issues associated with mechanical, electrical and thermal fields. Further investigation on the difference between the two-way coupled theory and the one-way coupled theory, referred to as the coupled model and the uncoupled model in this paper, and the relation between the two-way coupling effect and structural parameters, is necessary. The present paper employs the two-way coupled theory to model smart composite plates with surface-bonded piezoelectric layers. The higher order displacement theory is used to describe the displacement field to properly account for the transverse shear stresses that are important in anisotropic

1530-8138/00/03 0169-11 $10.00/0 DOI: 10.1106/50V9-519W-QVUV-AL7L

composites. The developed theory is therefore applicable to both thin and moderately thick constructions. A higher order potential field is developed to accurately describe the nonuniform distribution of electric field through the thickness of piezoelectric layers. The electric field distribution is now consistent with the induced effects due to the higher order displacement field. The governing equations are obtained based on the higher order field assumptions and variational principle of coupled fields. Numerical results are presented to investigate the difference between the coupled piezoelectric-mechanical model and the conventional uncoupled model. The actuation effects of actuators including multiple actuators, sensing ability of sensors and control authority, using the two-way coupled theory, are studied.

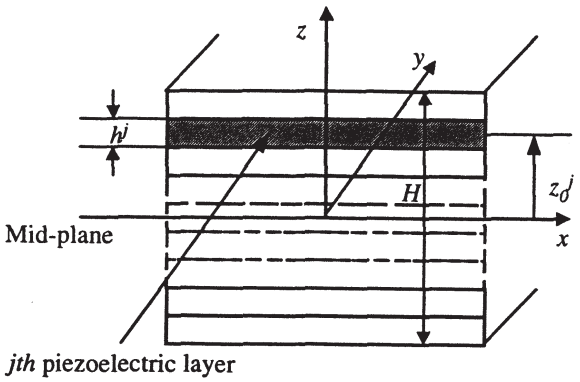

Figure 1. *Illustration of laminated element.*

MATHEMATICAL FORMULATION

In isothermal conditions, the linear electromechanical multiple field problem for a domain V without free body charge, based on displacement and electric potential as independent state variables, can be described using variational principle along with several constraints.

$$\delta\pi(u_i,\phi) = \int_{t_0}^{t} dt \left\{ \int_V (\rho \ddot{u}_i \delta u_i + \gamma \dot{u}_i \delta u_i + \sigma_{ij}\delta\varepsilon_{ij}) dV \right.$$

$$\left. - \int_V f_i \delta u_i dV - \int_{S_\sigma} \bar{t}_i \delta u_i dS - \int_V D_i \delta\phi_{,i} dV + \int_{S_D} \bar{q}\delta\phi dS \right\} = 0 \tag{1}$$

with constitutive relations

$$\sigma_{ij} = c_{ijkl}\varepsilon_{kl} - e_{ijk}E_k \tag{2}$$

$$D_i = e_{ijk}\varepsilon_{jk} + b_{ij}E_j \tag{3}$$

compatible conditions

$$\varepsilon_{ij} - \frac{1}{2}(u_{i,j} + u_{j,i}) = 0 \tag{4}$$

$$E_i + \phi_{,i} = 0 \tag{5}$$

and essential boundary conditions as follows:

$$u_i - \bar{u}_i = 0 \quad \text{on } S_u \tag{6}$$

$$\phi - \bar{\phi} = 0 \quad \text{on } S_\phi \tag{7}$$

where the quantities u_i, ε_{ij} and σ_{ij} denote the components of mechanical displacement, strain tensor and stress tensor, respectively and ϕ, E_i and D_i denote electric potential, and components of electric field and electric displacement, respectively. The quantities $\bar{u}_i, \bar{t}_i, \bar{\phi}$ and $\bar{q}$ denote the prescribed deformation on the displacement boundary S_u, traction on the stress boundary S_σ, voltage on the potential boundary S_ϕ and surface charge on the charge boundary S_D, respectively and ρ, γ and f_i denote mass density, structural damping and components of external force per unit volume, respectively. The quantities c_{ijkl}, e_{ijk} and b_{ij} represent elastic constants, piezoelectric constants and dielectric permittivity, respectively.

An accurate and effective field assumption of structural deformation and electric potential distribution is a key issue in the implementation of the variational principle into finite element governing equations. For laminated composite plates, the transverse shear effects are important due to the significant stiffness variation between different lamina. The assumed potential distribution is also required to describe the nonuniform potential distribution and match the field variation induced by mechanical deformation through piezoelectric effect. The equipotential requirements on the surfaces of piezoelectric transducers, the major electrical boundary condition, must be satisfied accurately. Therefore, the higher order assumptions for both displacement and electric potential are appropriate.

The displacement field is modeled using the higher order theory that incorporates the transverse shear effects. A laminated plate element with coordinate x-y-z is shown in Figure 1. Through the element thickness, cubic variations are assumed for in-plane displacements (u and v) and the out-of-plane displacement (w) is assumed constant. The following displacement field is obtained through the imposition of the zero transverse shear stress conditions on the surfaces of the laminate.

$$u(x,y,z) = u_0(x,y) - z\frac{\partial w_0(x,y)}{\partial x} + g(z,H)\psi_1(x,y) \tag{8}$$

$$v(x,y,z) = v_0(x,y) - z\frac{\partial w_0(x,y)}{\partial y} + g(z,H)\psi_2(x,y) \tag{9}$$

$$w(x,y,z) = w_0(x,y) \tag{10}$$

with

$$g(z, H) = z - \frac{4}{3H^2} z^3 \tag{11}$$

where u_0, v_0 and w_0 are the displacements of a point in the mid-plane of the laminate ($z = 0$). The terms $-z(\partial w_0/\partial x)$ and $-z(\partial w_0/\partial y)$ represent the effects of section rotations with respect to the y and $-x$ axes, respectively. The quantities ψ_1 and ψ_2 represent the mid-plane transverse shear strains and H indicates the distance between the laminate surfaces (Figure 1). The transverse shear effects are addressed by the higher order terms $g(z,H)\psi_1$ and $g(z,H)\psi_2$, which introduce the warping effects into the rigid rotation of plate sections.

A cubic distribution of the potential field (ϕ) along the thickness of piezoelectric layers is also assumed. The potential field must satisfy the surface boundary condition of applied voltages ($\bar{\phi}^j$). The potential field (ϕ^j) for the jth layer can be written as follows:

$$\phi^j(x, y, z) = \phi_0^j(x, y) - (z - z_0^j)E_z^j(x, y) + f(z - z_0^j, h^j)\left[(z - z_0^j)\left(\frac{\bar{\phi}^j}{h^j} + E_z^j(x, y)\right) - \phi_0^j(x, y)\right] \tag{12}$$

with

$$f(z - z_0^j, h^j) = 4\left(\frac{z - z_0^j}{h^j}\right)^2 \tag{13}$$

where ϕ_0^j is the potential of a point in the mid-plane of the jth piezoelectric layer. The quantity E_z^j denotes the electric field of mid-plane and the term $-(z - z_0^i)E_z^j$ is used to address the linear potential distribution along the thickness. The last term in Equation (12) represents the higher order modification addressing the nonuniform potential variation along the thickness and satisfying the equilpotential surface boundary conditions prescribed at electrodes. The quantity $\bar{\phi}^j$ denotes the potential difference between the top and the bottom electrodes covering the jth piezoelectric transducer and z_0^j and h^j denote the mid-plane position and the thickness of the jth piezoelectric layer, respectively (Figure 1).

The finite element governing equations are obtained by using the assumed field functions in the variational principle [Equation (1)]. The detailed procedure is illustrated in Appendix A. The element equilibrium equation is written as follows:

$$\begin{bmatrix} \mathbf{M}_{uu}^e & 0 \\ 0 & 0 \end{bmatrix} \begin{Bmatrix} \ddot{\mathbf{u}}_u^e \\ \ddot{\mathbf{u}}_\phi^e \end{Bmatrix} + \begin{bmatrix} \mathbf{C}_{uu}^e & 0 \\ 0 & 0 \end{bmatrix} \begin{Bmatrix} \dot{\mathbf{u}}_u^e \\ \dot{\mathbf{u}}_\phi^e \end{Bmatrix} + \begin{bmatrix} \mathbf{K}_{uu}^e & \lambda_e \mathbf{K}_{u\phi}^e \\ \lambda_e \mathbf{K}_{\phi u}^e & \lambda_e^2 \mathbf{K}_{\phi\phi}^e \end{bmatrix} \begin{Bmatrix} \mathbf{u}_u^e \\ \mathbf{u}_\phi^e / \lambda_e \end{Bmatrix} = \begin{Bmatrix} \mathbf{F}_u^e + \mathbf{F}_\Lambda^e \\ \lambda_e(\mathbf{F}_\phi^e + \mathbf{F}_p^e) \end{Bmatrix} \tag{14}$$

where $\mathbf{M}_{uu}^e$, $\mathbf{C}_{uu}^e$ and $\mathbf{K}_{uu}^e$ are mass, damping and stiffness matrices of the element, respectively. Matrix $\mathbf{K}_{\phi\phi}^e$ is the element electrical stiffness matrix and $\mathbf{K}_{u\phi}^e$ and $\mathbf{K}_{\phi u}^e$ are element stiffness matrices due to piezoelectric-mechanical couplings describing converse piezoelectric and piezoelectric effects, respectively. The external mechanical force vector is denoted $\mathbf{F}_u^e$ and the induced force vector due to applied potential is denoted $\mathbf{F}_\Lambda^e$. The electrical forces due to prescribed surface charge and applied voltage are denoted $\mathbf{F}_\phi^e$ and $\mathbf{F}_p^e$, respectively. The exact definitions of these matrices are presented in Appendix B.

The governing equation [Equation (14)] must be solved simultaneously after element assembly. A scaling parameter (λ_e) is introduced to avoid numerical problems due to scale differences between the stiffness matrices $\mathbf{K}_{uu}^e$, $\mathbf{K}_{u\phi}^e$ and $\mathbf{K}_{\phi\phi}^e$. This scaling parameter is chosen to make the magnitudes of the elements in the electrical components of the stiffness matrix roughly equal to the magnitudes in the mechanical components, $\mathbf{K}_{uu}^e$. Appropriate mechanical boundary conditions are used to eliminate rigid body motion. It must be noted that it is not necessary to impose boundary conditions on the electrical variables. This is due to the fact that the essential boundary conditions of the potentials, prescribed on the surfaces of piezoelectric layers, have been incorporated in the higher order potential assumption.

RESULTS AND DISCUSSION

Verification of the refined higher order laminate theory and the concept of simultaneously solving the coupled equations was previously made in earlier work (Chattopadhyay, Li, and Gu, 1999; Gu et al.; Zhou et al.) by comparison with the results from a 3-D model using ANSYS. The present paper, therefore, concentrates on the effects of the higher order potential function and the interaction between multiple actuators.

A cantilever rectangular fiber-reinforced laminated composite plate (Graphite/Epoxy) with surface-bonded piezoelectric transducers is considered in the numerical analysis (Figure 2). The plate dimensions are such that length a = 0.30 m and width b = 0.25 m. The stacking sequence is $[0°/90°]_s$. The material constants for the composite and the piezoelectric materials are listed in Table 1. The tip position of the structure is denoted point C (Figure 2). The plate structure is uniformly discretized into 49 four-noded plate elements. Several numerical cases are studied to evaluate the impact of coupling effects.

A comparison of piezoelectric actuation effect using the coupled model and the uncoupled model is performed. First, a plate with thickness h = 2 mm and top and bottom surface-bonded actuators (A/S1 and A/S2, Figure 2) is considered. The top and the bottom actuators are subjected to a static voltage of equal magnitude but opposite directions, making out-of-plane deformation dominant. It must be noted that the nominal electric field, defined as the value of the voltage ap-

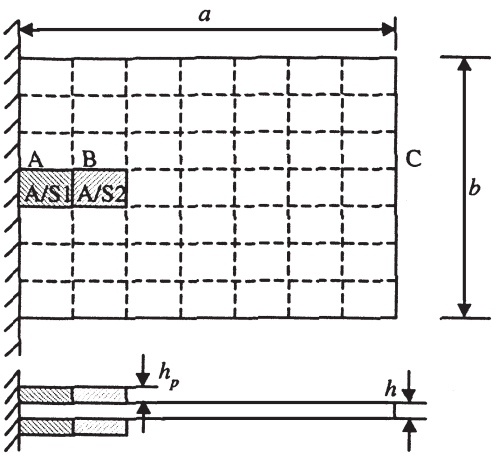

Figure 2. *Cantilever plate with actuators/sensors.*

plied on the actuator over its thickness (h_p, Figure 2) in the coupled model, is the same as the electric field used in the uncoupled model. In the following studies, the nominal electric field is maintained at 0.1 MV/m. The tip deflection of the plate (point C, Figure 2) is used to evaluate the actuation effect. The variation of tip deflection with change in the thickness ratio of actuator to plate structure is presented in Figure 3. It can be observed that initially the deflection increases with increase in the actuator-to-plate thickness ratio. However, the trend reverses with further increase in this ratio. This is due to the fact that increase in actuator thickness can enhance actuation force if the strain in actuators holds. However, thick actuator also increases bending stiffness greatly, which leads to smaller structural deformation. Therefore, there exists an optimized actuator-to-plate thickness ratio which can result in the largest deformation and thereby the largest actuation effect. In the example structure, both the coupled and the uncoupled theory predict the same optimized thickness ratio of about 1.1 (Figure 3). Though this thickness ratio results in the largest deflection, it is not always practical to implement. Unless the plate is rather thin, thickness ratios greater than about one will result in thick, heavy actuators. It can also be observed from Figure 3 that there is little difference in the values of tip deflection, between the two theories, if thin actuators are used. However, with increase in the actuator-to-plate thickness ratio, the difference between the predictions from two models becomes significant. The uncoupled theory predicts larger deformation compared to the coupled theory. This is because more transformation of mechanical energy into electrical energy due to the two-way coupling effect is considered in the coupled model. The uncoupled theory therefore overpredicts the control authority. This result has been proved in previous studies (Chattopadhyay, Li, and Gu, 1999; Gu et al.; Zhou et al.). To illustrate the significance of the actuator-to-plate thickness ratio, two plates with the same configuration as shown in Figure 2 and different thickness ($h = 2$ mm and $h = 0.4$ mm) are investigated. Figure 4 presents the difference in tip deflection by using the coupled and the uncoupled models. For both plates, little difference between the results from the two theories is observed with small values of actuator-to-plate thickness ratio. However, the thickness ratio of 1.1, the best geometry for actuation effects, yields the largest difference in deflections between the two models. Figure 5 presents the normalized difference in tip deflection by using the two models. Normalized difference is defined as the ratio of the difference between the deflections obtained using the two models to the deflection obtained using the uncoupled model. This ratio is used to evaluate the difference between the two theories. It can be observed that for both plates with different thickness, the normalized difference increases with increase in the actuator-to-plate thickness ratio. This results from the fact that the uncoupled model mispredicts the nonuniform distribution of electric field and the two-way interactions between electrical and mechanical fields more greatly in case of thick actuators. The normalized difference between the two models is about 5 percent in the cases studied for the actuator-to-plate thickness ratio of 1.1. It must be noted that the deviation between the two theories will vary with structural configurations and material properties. Larger piezoelectric coupling coefficients, implying more coupling energy stored in piezoelectric materials, will have the same effect as increased actuator-to-plate thickness ratio. This will also lead to more deviation between the predictions from the two models. The coupled theory will therefore be more appropriate in the modeling of newly developed high-actuation materials.

A plate thickness of 2 mm and the actuator-to-plate thickness ratio of 1.1 is used in the following investigations. The results presented for the coupled theory utilize the higher order potential distribution and the results for the uncoupled

Table 1. Material properties of PZT and graphite/epoxy composite.

	PZT	Graphite/Epoxy
Elastic moduli (GPa):		
E_{11}	63	144.23
E_{22}	63	9.65
E_{33}	63	9.65
Shear moduli (GPa):		
G_{23}	24.6	3.45
G_{13}	24.6	4.14
G_{12}	24.6	4.14
Poisson's ratio:		
ν	0.28	0.3
Density (kg/m^3):		
ρ	7600	1389.23
Piezoelectric charge constant (pm/V):		
$e_{31} = e_{32}$	253	—
Electric permittivity (nf/m):		
$b_{11} = b_{22}$	15.3	—
b_{33}	15.0	—
Curie temperature (°C):		
T_c	365	—

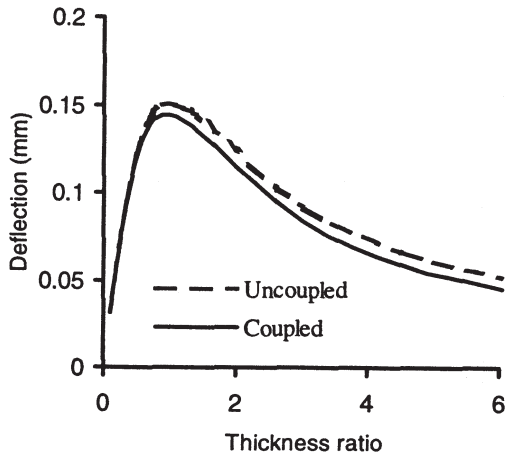

Figure 3. *Tip deflection with variation in actuator-to-plate thickness ratio (h_p /h).*

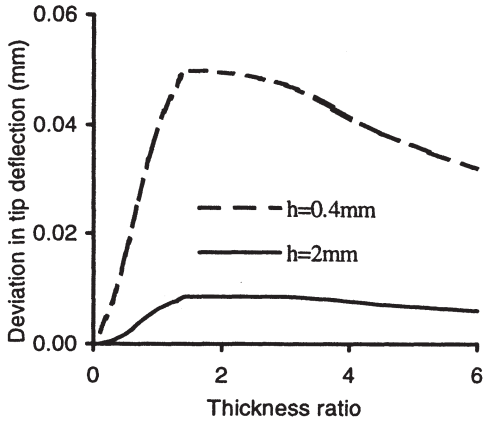

Figure 4. *Difference in tip deflection between coupled and uncoupled models, with variation in actuator-to-plate thickness ratio (h_p/h).*

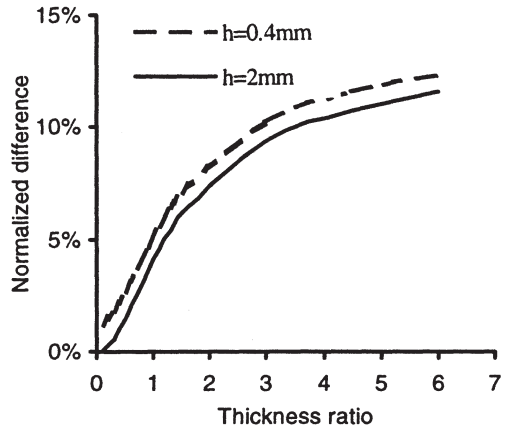

Figure 5. *Normalized difference in tip deflection, coupled and uncoupled models, with variation in actuator-to-plate thickness ratio (h_p /h).*

model use the standard linear description of the electric potential and thus constant electric field. Figure 6 presents potential and electric field distributions through the thickness of the top actuator, at point B, subjected to a nominal electric field of 0.1 MV/m. Note that the thickness coordinate of the actuator varies from 1.0 mm to 3.2 mm, that is, from the bottom surface to the top surface. The potential distribution obtained using the coupled theory and higher order potential field assumption deviates from the linear prediction in the uncoupled theory. Though the difference in the electric potentials is only a subtle curvature, this results in large divergence in electric fields obtained from the two models since the electric field is proportional to the slope of the potential. The deviation is a maximum at the actuator surfaces with about a 30 percent difference in electric field between the two models.

One significant effect of the deviation in electric field between the coupled and uncoupled models is the prediction of the charge accumulated on the surfaces of piezoelectric materials. Figure 7 presents the total charge accumulated on the actuator surfaces (A/S1 and A/S2, Figure 2). The coupled theory shows equal amount of charge on the top and the bottom electrodes. However, the uncoupled theory presents different charge values on the actuator surfaces, violating the conservative charge law. This is due to the incorrect assumption of constant electric field in the uncoupled model. Equation (3) shows that if the electric field is assumed to be constant while the strain varies through the thickness of the piezoelectric, then the electric displacement will not be constant through the thickness which is required to conserve charge. If it is desired to use the uncoupled model to estimate the actual charge on the electrodes then the magnitudes predicted for the electrodes could be averaged. For the example in Figure 7 this would yield a value of 7.15×10^{-6} Coulombs as opposed to 7.02×10^{-6} Coulombs predicted by the coupled model. The small difference between these values is a result of not simultaneously solving Equations (2) and (3) in the uncoupled model. Figures 8 and 9 present the deflection and the slope of the plate length (line AC, Figure 2). It is clearly seen that a deviation between the two theories exists for both deflection and slope. These results demonstrate the inaccuracy associated with the use of the one-way coupled theory for modeling piezoelectric actuators.

Next, stress analysis is performed to investigate the effects of two-way coupling. Figure 10 presents the distribution of normal stress, σ_x, through laminate thickness obtained using the coupled and uncoupled models for the structural element with piezoelectric actuator A/S2 (Figure 2). The stress distribution is obtained through Gaussian point averaging technique. It can be observed that the distribution of σ_x is discontinuous at the layer interfaces. The results obtained using the two theories do not show much difference in the host plate. However, significant deviation between the stress predictions, using the two theories, is observed in the region of surface-bonded piezoelectric actuator. The different predictions result from ignoring the two-way coupling effects and

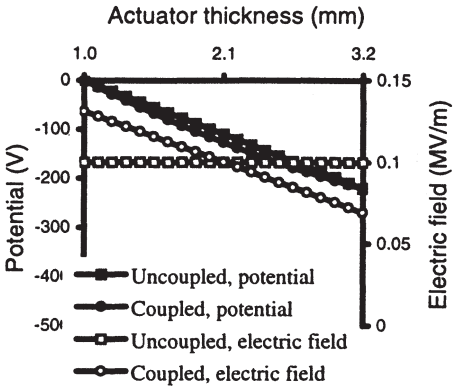

Figure 6. *Variations of potential and electric field through actuator thickness, coupled and uncoupled models.*

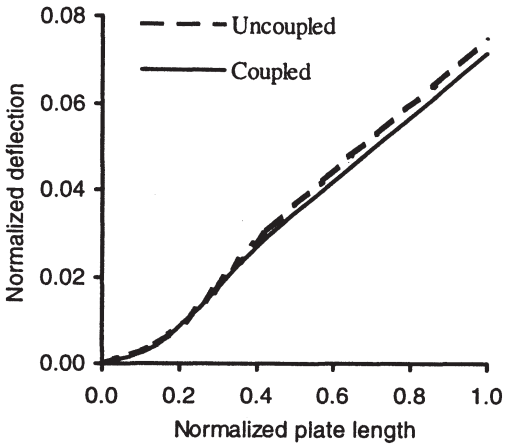

Figure 8. *Comparison of plate normalized deflection, coupled and uncoupled models.*

the constant electric field assumption in the uncoupled model. The electric field in the piezoelectric actuator is not uniformly distributed. For example, the magnitude of the electric field on the upper surface of the top actuator is greater compared to that on the lower surface, as shown in Figure 6. However, the uncoupled model uses the constant electric field assumption resulting in significant misprediction in electro-mechanical stress analysis. The largest deviation in stress prediction occurs on the actuator surfaces where the maximum deviation between the predictions of electric field using the two theories occurs. Figure 11 presents the distribution of normal stress, σ_y, through laminate thickness obtained using the coupled and uncoupled models for the structural element with piezoelectric actuator A/S2 (Figure 2). It can also be observed that there is a significant deviation between the stress evaluations using the two theories. The maximum deviation once again occurs at the actuator surfaces.

The effect of coupling on the transverse shear stress, σ_{xz}, is investigated in Figures 12–14. Figure 12 presents the distribution of stress σ_{xz} through laminate thickness obtained using the coupled and uncoupled models for the structural element with piezoelectric actuator A/S2 (Figure 2). It can be observed that both the coupled and the uncoupled models predict zero value at the top and bottom surfaces of the structure as expected. However, significant deviation occurs at the interface of the piezoelectric actuator and the host plate. The two theories also show difference in their predictions of the transverse shear stress distribution in x-y plane. The transverse shear stress σ_{xz} is evaluated at the midplane of the top actuator ($z = 2.1$mm) as well as at six different sections in the structural element A/S2 as shown in Figure 13. The comparison of stress σ_{xz} on the six sections is presented in Figure 14. Although the two theories yield similar trends in the stress variations, significant differences between the two theories can be observed. Note that the other shear stresses are not investigated since they are not as significant in the case studied here.

In practical applications, multiple actuators are used to produce larger actuation capability for both shape control and control of different vibration modes. The effect of the two-way coupling on multiple actuators is investigated in Figures 15 and 16. A plate thickness of 2 mm and actuator-to-plate thickness ratio of 1.1 is used. Four cases with different numbers of actuators are considered as shown in Figure 15. The change in number of actuator implies change in structural surface areas covered by actuators. A nominal electric

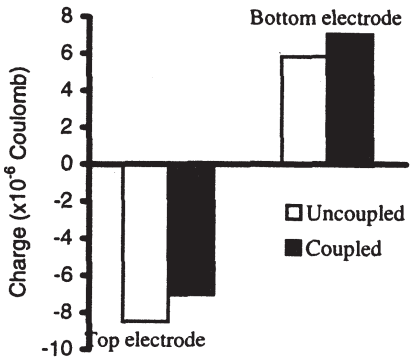

Figure 7. *Electric charge, top actuator.*

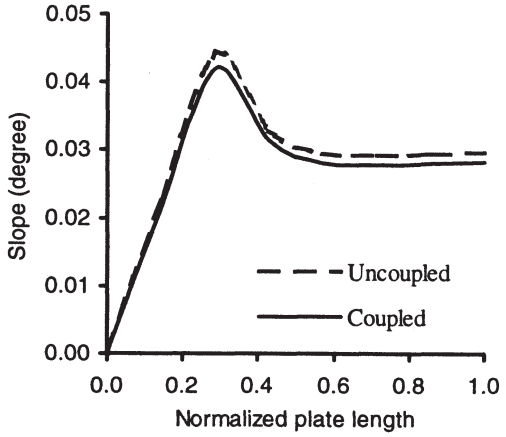

Figure 9. *Comparison of plate slope, coupled and uncoupled models.*

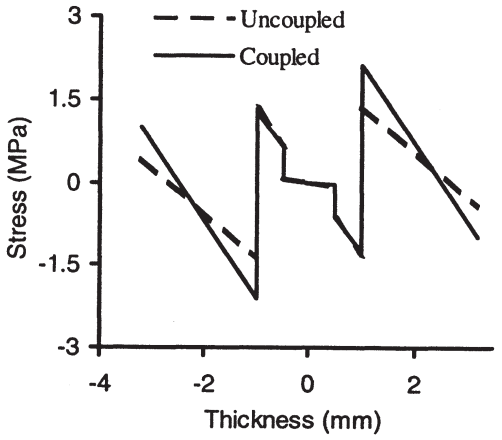

Figure 10. *Comparison of stress distribution (σ_x) through thickness, coupled and uncoupled models.*

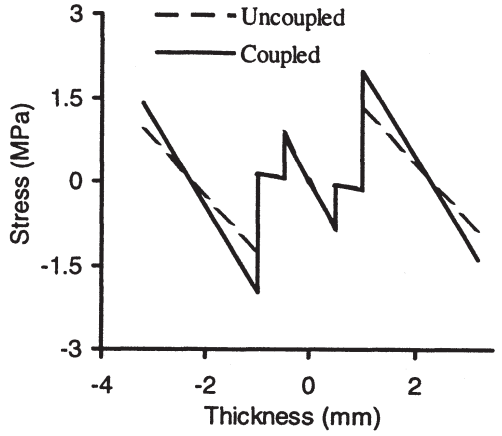

Figure 11. *Comparison of stress distribution (σ_y) through thickness, coupled and uncoupled models.*

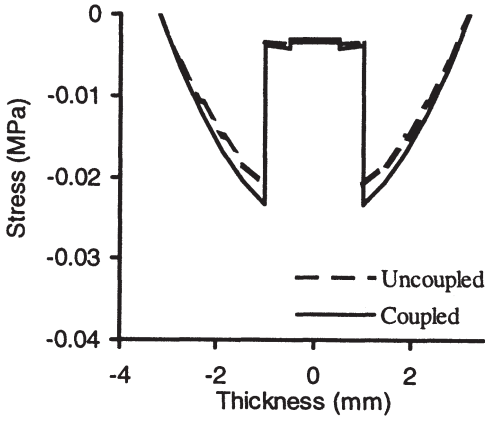

Figure 12. *Comparison of stress distribution (σ_{xz}) through thickness, coupled and uncoupled models.*

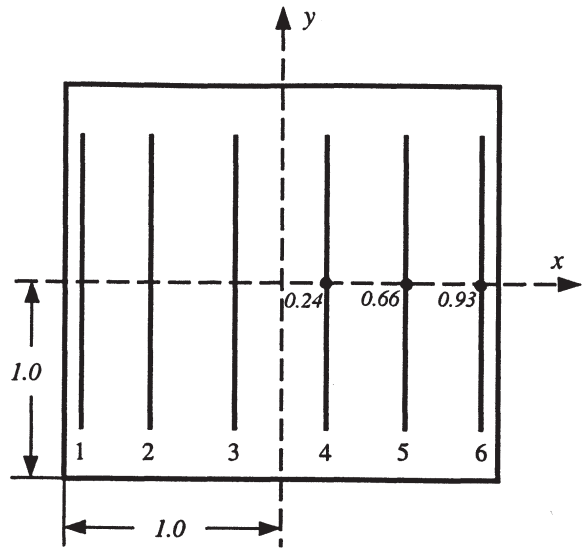

Figure 13. *Isoparametric illustration of sections in actuator element.*

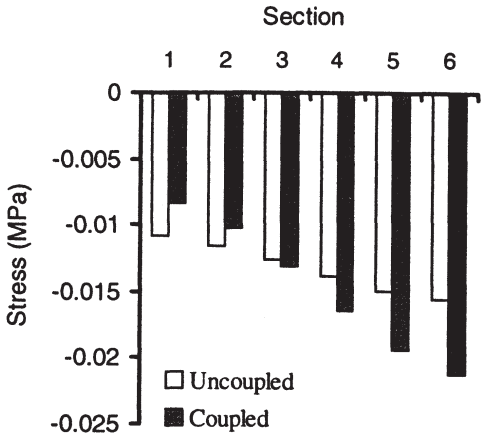

Figure 14. *Comparison of transverse shear stress distribution in x-y plane.*

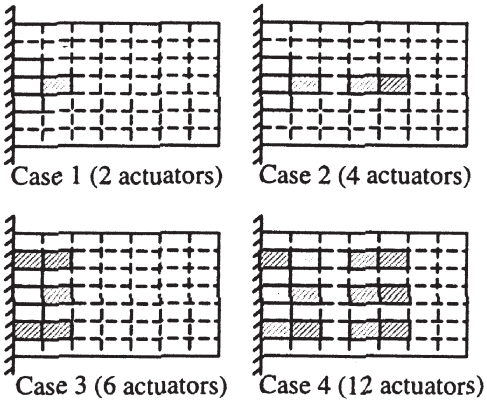

Figure 15. *Illustration of multiple actuator cases.*

field of 0.1 MV/m is applied in each case. The tip deflection normalized by the plate thickness (h, Figure 2) is used to evaluate the actuation effects. Comparisons of the normalized tip deflections, for all cases, are presented in Figure 16. As expected, both the uncoupled and the coupled theory predict larger tip deflection with increase in the number of actuator. However, the uncoupled theory results in larger deformation. The normalized differences between the two theories, for these four cases, are 4.8, 5.0, 5.2 and 5.4 percent, respectively. This indicates that the deviation between the two theories varies marginally with increase in the structural surface area covered by actuators or with change in actuator position. This can be explained as follows. The difference between the predictions from the two models results from piezoelectric effect, which is neglected if the uncoupled theory is used. The energy transferred from mechanical field to electrical field and stored in piezoelectric materials is ignored in the uncoupled model. Therefore, the deviation between the two models depends on the ratio of electrical energy stored in piezoelectric materials to mechanical energy stored in the structure. The energy misprediction by the uncoupled theory increases with increase in this ratio, resulting in increased deviation between the two theories. For the structure deformed by piezoelectric actuation, the higher strain region, representing larger mechanical energy stored, is concentrated in the region with piezoelectric actuators. Increase in the number of actuator will increase electrical energy stored in piezoelectric materials. However, this also implies increase in regions of high strain in the structure which leads to more mechanical energy in the deformed structure. Thus, increase in the number of actuator or change in actuator position does not affect the ratio of electrical to mechanical energy and therefore has marginal effect on the deviation between the two models.

Numerical analysis is performed to investigate piezoelectric sensing effects. The same cantilever plate with thickness of 2 mm and the thickness ratio of 1.1 is considered. The surface-bonded piezoelectric elements A/S1 and A/S2 are used as sensors (Figure 2). Figure 17 presents the potential and the electric field distributions through the thickness of the top sensor, at point B, due to the static deformation of the plate structure with a tip deflection of 5 mm. In the uncoupled model, the potential and the electric field are assumed zero as shown in Figure 17. The coupled model predicts nonzero values, which are induced by the mechanical deformation. The largest deviation of potential and electric field occur in the mid-plane and the surfaces of sensors, respectively. Figures 18 and 19 present the variations of charge accumulated on the top and the bottom electrodes, with time, respectively when the structure is released from the initial deformed state. It can be observed that the summation of charge variations on the two electrodes predicted by the coupled theory is zero, which implies charge conservation. However, the prediction from the uncoupled theory results in overestimation of the charge on the top electrode and underestimation of the charge on the bottom electrode.

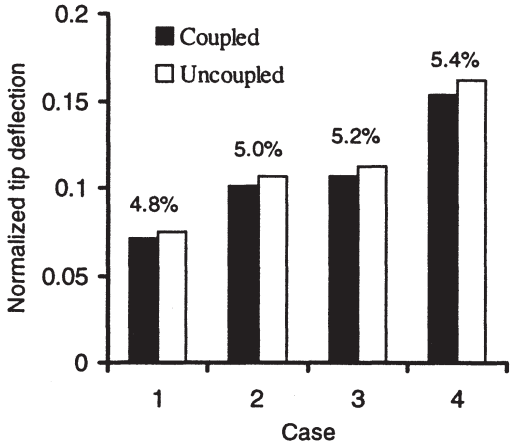

Figure 16. *Comparison of normalized tip deflections.*

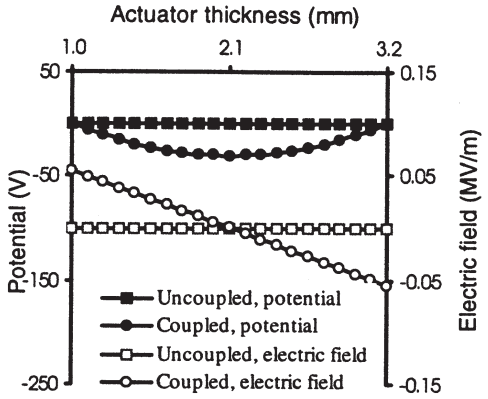

Figure 17. *Variations of potential and electric field through sensor thickness, coupled and uncoupled models.*

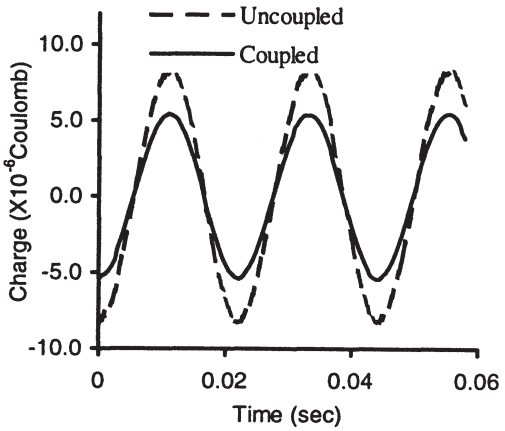

Figure 18. *Charge variation, top electrode, coupled and uncoupled models.*

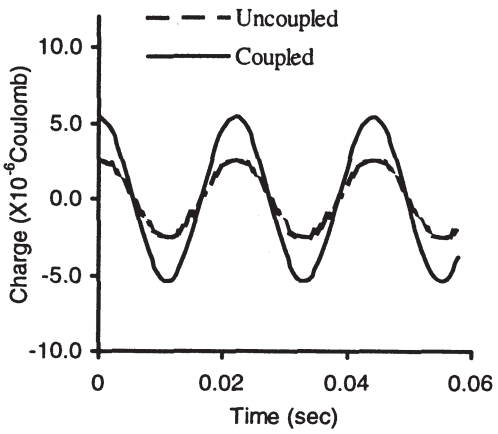

Figure 19. *Charge variation, bottom electrode, coupled and uncoupled models.*

CONCLUDING REMARKS

A completely coupled piezoelectric-mechanical theory, based on a higher order displacement field and a higher order electric potential field, is developed to study the coupling effects of piezoelectric smart composite plates. The governing equations are obtained using the higher order field assumptions and variational principle of coupled fields. The theory is implemented using finite element technique that ensures the application to practical geometry and boundary conditions. Numerical results are presented for a cantilever composite plate with piezoelectric transducers. The following important observations are made from this study.

1. The developed approach provides a means to accurately model the behavior of composite plates with piezoelectric actuators and sensors.
2. For surface-bonded actuators, the difference between the two theories is affected by a critical parameter, the thickness ratio of actuator to plate structure. Increase in this ratio leads to rapid increase in the deviation between the two theories.
3. Two-way coupling affects stress distribution significantly. The maximum deviation between stress predictions using the coupled and uncoupled theories occur at the top or the bottom surface of the piezoelectric layers.
4. For laminated plates with multiple surface-bonded actuators, the normalized difference between the two models is not sensitive to the number and the position of actuators.
5. The uncoupled model neglects the nonzero electric field induced by mechanical deformation in sensor applications. This leads to a violation of the conservative charge law. Furthermore, it also mispredicts the charge accumulated on electrodes significantly.
6. Difference in the predictions by the two models is not sensitive to increase in actuator size or number.

ACKNOWLEDGMENT

The research is supported by NASA Langley Research Center, grant number NAG-1-1988, technical monitor Carol D. Wieseman.

APPENDIX A

The finite element formulation of an n-noded element with m piezoelectric layers is considered. In-plane coordinates are denoted x and y and the thickness coordinate is denoted z. The position of the mid-plane of the jth piezoelectric layer is denoted z_0^j (Figure 1).

The nodal unknowns of displacement field for the ith node ($\mathbf{u}_u^i$) and electrical field for the ith node in the jth piezoelectric layer ($\mathbf{u}_\phi^{i,j}$) are written as follows.

$$\mathbf{u}_u^i = \left[u_0^i, v_0^i, w_0^i, \frac{\partial w_0^i}{\partial x}, \frac{\partial w_0^i}{\partial y}, \Psi_1^i, \Psi_2^i\right] \tag{A-1}$$

$$\mathbf{u}_\phi^{i,j} = [\phi_0^{i,j}, E_z^{i,j}] \tag{A-2}$$

The displacement ($\mathbf{u}_u^e$) and the jth layer electrical unknowns ($\mathbf{u}_\phi^{e,j}$) for the element e are written as follows.

$$\mathbf{u}_u^e = [\mathbf{u}_u^1, \mathbf{u}_u^2, \cdots, \mathbf{u}_u^n]^T \tag{A-3}$$

$$\mathbf{u}_\phi^{e,j} = [\mathbf{u}_\phi^{1,j}, \mathbf{u}_\phi^{2,j}, \cdots, \mathbf{u}_\phi^{n,j}]^T \tag{A-4}$$

The displacement field in the mid-plane of the element ($\mathbf{u}_{u0}(x,y)$) and the electrical field in the mid-plane of the jth piezoelectric layer ($\mathbf{u}_{\phi 0}^j(x, y)$) are,

$$\mathbf{u}_{u0}(x, y) = \left[u_{10}, v_{10}, w_{10}, \Psi_1, \Psi_2\right]^T \tag{A-5}$$

$$\mathbf{u}_{\phi 0}^j(x, y) = [\phi_0^j, E_z^j]^T \tag{A-6}$$

By using appropriate interpolation functions, the mid-plane field functions can be written as follows.

$$\mathbf{u}_{u0}(x, y) = \mathbf{N}_u(x, y)\mathbf{u}_u^e \tag{A-7}$$

$$\mathbf{u}_{\phi 0}^j(x, y) = \mathbf{N}_\phi(x, y)\mathbf{u}_\phi^{e,j} \tag{A-8}$$

where $\mathbf{N}_u(x,y)$ and $\mathbf{N}_\phi(x,y)$ are the interpolation functions for displacement and potential field, respectively.

Based on the higher order field assumption, the element displacement field $\mathbf{u}(x,y,z)$, the strain $\varepsilon(x,y,z)$, the potential field $\phi^j(x,y,z)$ and the electric field $\mathbf{E}^j(x,y,z)$ can be written as follows.

$$\mathbf{u}(x, y, z) = \mathbf{L}_u\mathbf{u}_{u0}(x, y) \tag{A-9}$$

$$\varepsilon(x,y,z) = \mathbf{L}_\varepsilon \mathbf{u}_{u0}(x,y) \tag{A-10}$$

$$\phi^j(x,y,z) = V_b(z - z_0^j, h^j, \bar{\phi}^j) + \mathbf{L}_\phi^j \mathbf{u}_{\phi 0}^j(x,y) \tag{A-11}$$

$$-\mathbf{E}^j(x,y,z) = \mathbf{F}_b(z - z_0^j, h^j, \bar{\phi}^j) + \mathbf{L}_E^j \mathbf{u}_{\phi 0}^j(x,y) \tag{A-12}$$

where the higher order operators $\mathbf{L}_u$, $\mathbf{L}_\varepsilon$, $\mathbf{L}_\phi^j$ and $\mathbf{L}_E^j$ are defined as follows.

$$\mathbf{L}_u = \begin{bmatrix} 1 & 0 & -z\dfrac{\partial}{\partial x} & g(z,H) & 0 \\ 0 & 1 & -z\dfrac{\partial}{\partial y} & 0 & g(z,H) \\ 0 & 0 & 1 & 0 & 0 \end{bmatrix} \tag{A-13}$$

$$\mathbf{L}_\varepsilon = \begin{bmatrix} \dfrac{\partial}{\partial x} & 0 & -z\dfrac{\partial^2}{\partial x^2} & g(z,H)\dfrac{\partial}{\partial x} & 0 \\ 0 & \dfrac{\partial}{\partial y} & -z\dfrac{\partial^2}{\partial y^2} & 0 & g(z,H)\dfrac{\partial}{\partial y} \\ 0 & 0 & 0 & 0 & \dfrac{\partial g(z,H)}{\partial z} \\ 0 & 0 & 0 & \dfrac{\partial g(z,H)}{\partial z} & 0 \\ \dfrac{\partial}{\partial y} & \dfrac{\partial}{\partial x} & -2z\dfrac{\partial^2}{\partial x \partial y} & g(z,H)\dfrac{\partial}{\partial y} & g(z,H)\dfrac{\partial}{\partial x} \end{bmatrix} \tag{A-14}$$

$$\mathbf{L}_\phi^j = h_1(z - z_0^j, h^j)\left\lfloor 1, -(z - z_0^j) \right\rfloor \tag{A-15}$$

$$\mathbf{L}_E^j = \begin{bmatrix} h_1(z - z_0^j, h^j)\dfrac{\partial}{\partial x} & h_2(z - z_0^j, h^j)\dfrac{\partial}{\partial x} \\ h_1(z - z_0^j, h^j)\dfrac{\partial}{\partial y} & h_2(z - z_0^j, h^j)\dfrac{\partial}{\partial y} \\ \dfrac{\partial h_1(z - z_0^j, h^j)}{\partial z} & \dfrac{\partial h_2(z - z_0^j, h^j)}{\partial z} \end{bmatrix} \tag{A-16}$$

with

$$V_b(z - z_0^j, h^j, \bar{\phi}^j) = \frac{(z - z_0^j)\bar{\phi}^j}{h^j} f(z - z_0^j, h^j) \tag{A-17}$$

$$\mathbf{F}_b(z - z_0^j, h^j, \bar{\phi}^j) = \begin{bmatrix} 0 \\ 0 \\ \dfrac{12\bar{\phi}^j}{(h^j)^3}(z - z_0^j)^2 \end{bmatrix} \tag{A-18}$$

$$h_1(z - z_0^j, h^j) = 1 - f(z - z_0^j, h^j) \tag{A-19}$$

$$h_2(z - z_0^j, h^j) = -(z - z_0^j) h_1(z - z_0^j, h^j) \tag{A-20}$$

The element displacement field, the strain, the potential field and the electric field can be written as follows.

$$\mathbf{u}(x,y,z) = \mathbf{B}_u \mathbf{u}_u^e \tag{A-21}$$

$$\varepsilon(x,y,z) = \mathbf{B}_\varepsilon \mathbf{u}_u^e \tag{A-22}$$

$$\phi^j(x,y,z) = V_b(z - z_0^j, \bar{\phi}^j) + \mathbf{B}_\phi \mathbf{u}_\phi^{e,j} \tag{A-23}$$

$$-\mathbf{E}^j(x,y,z) = \mathbf{F}_b(z - z_0^j, h^j, \bar{\phi}^j) + \mathbf{B}_E^j \mathbf{u}_\phi^{e,j} \tag{A-24}$$

where

$$\mathbf{B}_u = \mathbf{L}_u \mathbf{N}_u(x,y) \tag{A-25}$$

$$\mathbf{B}_\varepsilon = \mathbf{L}_\varepsilon \mathbf{N}_u(x,y) \tag{A-26}$$

$$\mathbf{B}_\phi^j = \mathbf{L}_\phi^j \mathbf{N}_\phi(x,y) \tag{A-27}$$

$$\mathbf{B}_E^j = \mathbf{L}_E^j \mathbf{N}_\phi(x,y) \tag{A-28}$$

The constitutive relations in vector form are as follows:

$$\boldsymbol{\sigma} = \mathbf{Q}\boldsymbol{\varepsilon} - \mathbf{P}\mathbf{E} \tag{A-29}$$

$$\mathbf{D} = \mathbf{P}^T\boldsymbol{\varepsilon} + \mathbf{B}\mathbf{E} \tag{A-30}$$

where $\boldsymbol{\sigma}$ and $\mathbf{D}$ are the stress vector and the electric displacement vector, respectively and $\boldsymbol{\varepsilon}$ and $\mathbf{E}$ are the strain vector and the electric field vector, respectively. The matrices $\mathbf{Q}$, $\mathbf{B}$ and $\mathbf{P}$ denote elastic constants, dielectric permittivity and piezoelectric constants, respectively.

Substitution of Equations (A-25)–(A-28) into the variational principle yields the element governing equation [Equation (14)]. The element matrices are defined in Appendix B.

APPENDIX B

Element matrices in Equation (14) are defined as follows.

$$\mathbf{M}_{uu}^e = \int_V \mathbf{B}_u^T \rho \mathbf{B}_u dV \tag{B-1}$$

$$\mathbf{C}_{uu}^e = \int_V \mathbf{B}_u^T \gamma \mathbf{B}_u dV \tag{B-2}$$

$$\mathbf{K}_{uu}^e = \int_V \mathbf{B}_\varepsilon^T \mathbf{Q} \mathbf{B}_\varepsilon dV \tag{B-3}$$

$$\mathbf{K}^e_{u\phi} = \left[\int_{V^1} \mathbf{B}^T_\varepsilon \mathbf{P}^1 \mathbf{B}^1_E dV, \cdots, \int_{V^m} \mathbf{B}^T_\varepsilon \mathbf{P}^m \mathbf{B}^m_E dV\right] \quad \text{(B-4)}$$

$$\mathbf{F}^e_u = \int_V \mathbf{B}^T_u \mathbf{f} dV + \int_S \mathbf{B}^T_u \mathbf{t} dS \quad \text{(B-5)}$$

$$\mathbf{F}^e_A = -\sum_{j=1}^{m} \int_{V^j} \mathbf{B}^T_\varepsilon \mathbf{P}^j \mathbf{F}_b(z - z^j_0, h^j, \bar{\phi}^j) dV \quad \text{(B-6)}$$

$$\mathbf{K}^e_{\phi u} = -\mathbf{K}^{eT}_{u\phi} \quad \text{(B-7)}$$

$$\mathbf{K}^e_{\phi\phi} = \begin{bmatrix} \int_{V^1} \mathbf{B}^{1T}_E \mathbf{B}^1 \mathbf{B}^1_E dV & \cdots & 0 \\ \cdots & \cdots & \cdots \\ 0 & \cdots & \int_{V^m} \mathbf{B}^{mT}_E \mathbf{B}^m \mathbf{B}^m_E dV \end{bmatrix} \quad \text{(B-8)}$$

$$\mathbf{F}^e_p = -\begin{bmatrix} \int_{V^1} \mathbf{B}^{1T}_E \mathbf{B}^1 \mathbf{F}_b(z - z^1_0, h^1, \bar{\phi}^1) dV \\ \cdots \\ \int_{V^m} \mathbf{B}^{mT}_E \mathbf{B}^m \mathbf{F}_b(z - z^m_0, h^m, \bar{\phi}^m) dV \end{bmatrix} \quad \text{(B-9)}$$

$$\mathbf{F}^e_\phi = -\begin{bmatrix} \int_{S^1} \mathbf{B}^{1T}_\phi q^1 dS \\ \cdots \\ \int_{S^m} \mathbf{B}^{mT}_\phi q^m dS \end{bmatrix} \quad \text{(B-10)}$$

where **f** and **t** denote body force vector per unit volume and surface traction vector, respectively. The superscripts 1 to *m* denote corresponding piezoelectric layers.

REFERENCES

Anderson, E. H. and Hagood, N. W. 1994. "Simultaneous Piezoelectric Sensing/Actuation: Analysis and Application to Controlled Structures," *Journal of Sound and Vibration*, 174(5):617–639.

Chattopadhyay, A. and Gu, H. 1994. "New Higher Order Plate Theory in Modeling Delamination Buckling of Composite Laminates," *AIAA Journal*, 32(8):1709–1716.

Chattopadhyay, A., Gu, H. and Dragomir-Daescu, D. 1999. "Dynamic of Delaminated Composite Plates with Piezoelectric Actuators," *AIAA Journal*, 37(2):248–254.

Chattopadhyay, A., Li, J., and Gu, H., "Coupled Thermo-Piezoelectric-Mechanical Model for Smart Composite Laminates," *AIAA Journal*, Vol. 37, No. 12, 1999, pp. 1633–1638.

Chattopadhyay, A. and Seeley, C. E. 1997. "A Higher Order Theory for Modeling Composite Laminates with Induced Strain Actuators," *Composite Part B Engineering*, 28B:243–252.

Cho, M. and Parmerter, R. R. 1993. "Efficient Higher Order Composite Plate Theory for General Lamination Configurations," *AIAA Journal*, 31(7):1299–1306.

Crawley, E. F. 1987. "Use of Piezoelectric Actuators as Elements of Intelligent Structures," *AIAA Journal*, 25(10):1373–1385.

Detwiler, D. T., Shen, M. H. and Venkayya, V. B. 1995. "Finite Element Analysis of Laminated Composite Structures Containing Distributed Piezoelectric Actuators and Sensors," *Finite Elements in Analysis and Design*, 20(2):87–100.

Gu, H., Chattopadhyay, A., Li, J. and Zhou, X. "A Higher Order Temperature Theory for Coupled Thermo-Piezoelectric-Mechanical Modeling of Smart Composites," (*International Journal of Solids and Structures*, in press).

Hagood, N. W. and Von Flotow, A. 1991. "Damping of Structural Vibrations with Piezoelectric Materials and Passive Electrical Networks," *Journal of Sound and Vibration*, 146(2):243–268.

Lee, C. K. 1990. "Theory of Laminated Piezoelectric Plates for the Design of Distributed Sensors/Actuators. Part I: Governing Equations and Reciprocal Relationships," *Journal of the Acoustical Society of America*, 87(3):1144–1158.

McCarthy, T. R and Chattopadhyay, A. 1997. "A Refined Higher Order Composite Box Beam Theory," *Composite Part B Engineering*, 28B: 523–534.

Mitchell, J. A. and Reddy, J. N. 1995. "A Refined Hybrid Plate Theory for Composite Laminates with Piezoelectric Laminae," *International Journal of Solids and Structures*, 32(16):2345–2367.

Tiersten, H. F. 1969. *Linear Piezoelectric Plate Vibrations.* Plenum, New York.

Zhou, X., Chattopadhyay, A. and Gu, H. "Dynamic Responses of Smart Composites Using A Coupled Thermo-Piezoelectric-Mechanical Model," (*AIAA Journal*, in press).